Proc. NIPR Symp. Polar Meteorol. Glaciol., 9, 87–109, 1995

NUMERICAL SIMULATION OF SHIRASE GLACIER, EAST QUEEN MAUD LAND, ANTARCTICA

Frank PATTYN and Hugo DECLEIR

Department of Geography, Vrije Universiteit Brussel, Pleinlaan 2, B-1050 Brussels, Belgium

Abstract: Recent observations in Shirase Drainage Basin, East Queen Maud Land, Antarctica show that the ice sheet is thinning at a considerable rate and that this thinning started about a few thousand years ago. In order to improve insight into the present transient behavior of the ice sheet in Shirase Drainage Basin, a two-dimensional time-dependent flow line model was developed. The ice sheet system model takes into account a coupled ice shelf, longitudinal stress in the ice sheet and grounding zone domain, basal sliding and local isostatic bedrock adjustment. The two-dimensional temperature field is fully coupled to the velocity field. The model is numerically solved on a fine grid, which is unequally spaced both in the horizontal and the vertical directions. By simulating the evolution of the ice sheet during a complete glacial-interglacial cycle it was possible to obtain better insight into the reaction of the ice sheet to environmental changes (temperature, sea-level and mass balance) and to calculate the present local imbalance. Investigation of the role of geothermal heating at the ice sheet base showed that changes in geothermal heat flux and the inclusion of bedrock heating did not alter significantly the overall ice sheet geometry. The dynamical experiments revealed that the present modeled imbalance is much lower than the observed rate of change. Also, a significant discrepancy between the observed and the modeled surface velocities in the stream area could point to a model deficiency in treating the present ice dynamics at the grounding line and the ice tongue. Since the modeled ice dynamics at Mizuho Plateau are more or less in accord with the observed dynamics, we are of the opinion that changes in the dynamic behavior of the ice stream area are a possible cause for the enhanced ice sheet thinning.

1. Introduction

Whether the Antarctic ice sheet is a stable or more dynamic feature on the surface of the earth, environmental changes may have a drastic impact on the local behavior of the ice cap. The marine ice streams, prevalent over West Antarctica, show at present much dynamism and may be subject to considerable volume changes as caused by climatic changes, both in the past as in the future. The East Antarctic ice sheet on the other hand seems to be of more stable nature (DENTON *et al.*, 1993; HUYBRECHTS, 1993). Nevertheless, a few large outlet glaciers (also called continental ice streams), such as Lambert Glacier and Jutulstraumen, drain a considerable amount of ice directly into the ocean. The reaction of these outlet glaciers to climatic change is thus of great importance in investigating the overall stability and regional ice dynamics of the East Antarctic ice sheet.

In this paper we will focus on Shirase Glacier (70° S, 39° E) in East Queen Maud Land (Fig. 1). This important continental ice stream drains about 90% of the total ice

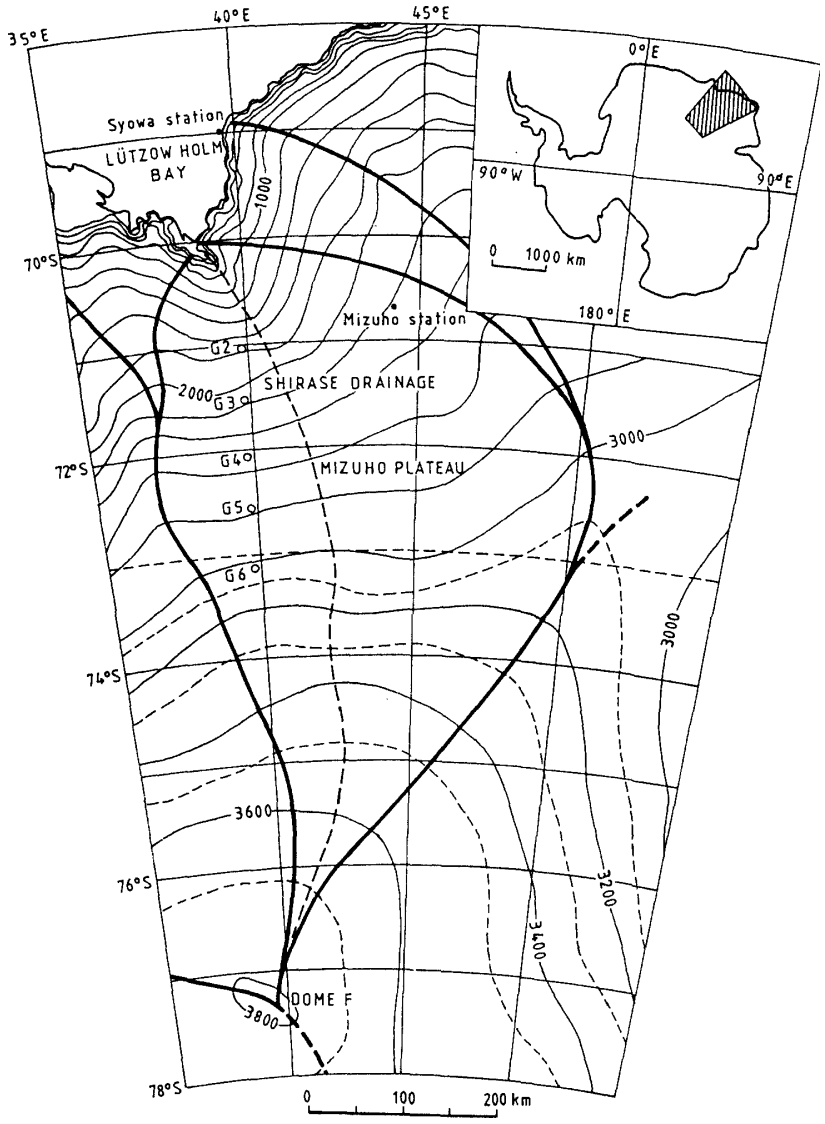

Fig. 1. Location map of Shirase Drainage Basin in East Queen Maud Land. The dashed line represents the central flow line, as primary input for the modeling experiments in this paper. The flow line starts at Dome Fuji, follows more or less the 40°E meridian towards Lützow-Holm Bay, and ends at Shirase Glacier in a floating ice tongue. Also displayed are stations G2 to G6 where ice thickness and velocity measurements were carried out (NISHIO et al., 1989).

discharge of Shirase Drainage Basin covering approximately 200000 km^2 of ice coming from the polar plateau near Dome Fuji (77°22′ S, 39°37′ E) (FUJII, 1981). Shirase Glacier is the second major outlet glacier (after Lambert Glacier) in this region and one of the fastest Antarctic glaciers, with velocities up to 2700 m a^{-1} in the stream region (FUJII, 1981). Shirase Glacier covers a wide valley, which curves from the northward direction near the exit area to the north-west direction further inland. The subglacial bedrock lies below sea level at a distance of 100 km from the present coastline to reach 500 m a.s.l. near Mizuho Plateau (MAE and YOSHIDA, 1987). Elsewhere, the bedrock lies between 500 and 1000 m a.s.l. The glacier terminus is a free floating ice tongue in

Lützow-Holm Bay. The shallow continental platform (< -300 m a.s.l.) in the eastern part of this bay is characterized by drowned glacial troughs. The "Central Trough" extends up to 100 km northward from Shirase Glacier and reaches locally (close to Shirase Glacier) -1600 m a.s.l. (MORIWAKI and YOSHIDA, 1983). The location of these troughs seems, as elsewhere in Antarctica, to be controlled by tectonics. The ice flow in Shirase Drainage Basin is also characterized by large convergence toward the Shirase Glacier stream area.

Extensive field work has been carried out in Shirase Drainage Basin during the last three decades. During the Japanese Glaciological Research Program (1969-1975), its major aim being the study of the ice flow of Mizuho Plateau, repetitive surveying of a triangulation chain, 250 km in length, revealed large submergence velocities (0.7 to 1.0 m a^{-1}) in the region along the 72°S parallel, from 39°E to 43°E (NARUSE, 1979). Taking into account densification in the upper firn layers, the accumulation was not enough to compensate for the ice mass deficit caused by the submergent flow, hence substantial thinning of the ice sheet at Mizuho Plateau was inferred. Later measurements in this area (NISHIO *et al.*, 1989; TOH and SHIBUYA, 1992) confirmed this thinning rate ranging from 0.5 to 2.0 m a^{-1} in the region where the surface elevation is lower than 2800 m. Furthermore, from an analysis of the total gas content of ice cores in Mizuho Plateau (KAMEDA *et al.*, 1990) it was also found that the ice sheet decreased by 350 m during the last 2000 years, and it was concluded that the thinning is a rather recent phenomenon. MAE and NARUSE (1978) and MAE (1979) argue that the thinning of the ice sheet in this particular area is predominantly caused by basal sliding with a velocity of about 10 m a^{-1}. These conclusions were drawn by applying the mass continuity equation (in a simplified version) to the local ice configuration properties, such as local ice thickness, surface and bedrock gradient, surface strain-rates, and mass balance. In addition the calculation of the basal shear stress profile along the central flow line was found to be similar to the shear stress profile of surging glaciers (MAE, 1979). This led the authors to conclude that the ice sheet is not in a steady state. However, no field survey data on the basal sliding velocity are available, nor is there new evidence supporting the thesis that the basal sliding mechanism is the main cause of enhanced ice sheet thinning.

It is however very likely that basal sliding will occur. Radio echo sounding in Shirase Drainage Basin (NISHIO and URATSUKA, 1991) shows that large areas in the lower drainage basin are characterized by pressure melting at the base, and the authors estimated a water layer thickness of 0-30 cm at the interface between the base of the ice sheet and the bedrock in the downstream area of Shirase Glacier, even in areas where the bedrock lies well above sea level. Basal sliding is thus a candidate in playing a major role in the dynamic behavior of the ice sheet at Mizuho Plateau and certainly in the downstream area.

Despite the abundance of field data, numerical modeling experiments in the Shirase Drainage Basin area are very scarce. Apart from some steady state temperature and glacier profile reconstructions (NISHIO *et al.*, 1989), three-dimensional dynamic modeling was performed by NAGAO *et al.* (1984) and with an improved finite element model by FUJITA *et al.* (1991). Despite this improvement, major shortcomings were the ignorance of longitudinal stress and isostatic changes, a fixed seaward boundary, and the

use of a steady state temperature profile. Excluding these features may seriously hamper a profound analysis of the ice sheet dynamics. Therefore, we developed an ice sheet system model, based on previous modeling experiments of Antarctic outlet glaciers (PATTYN *et al.*, 1989, 1992), but with a higher degree of sophistication. Modeling experiments, described in this paper, aim at a better understanding of the present ice sheet dynamics of Shirase Glacier, the sensitivity of the ice sheet system with respect to different boundary conditions and its dynamic behavior during the course of the last glacial-interglacial period.

2. Model Description

The numerical ice sheet system model used in this study is a dynamic flow line model that predicts the ice thickness distribution along a flow line in space and time as well as the two-dimensional flow regime (velocity, strain-rate and stress fields) and temperature distribution in response to environmental conditions. Since longitudinal stresses play an important role in large outlet glaciers and ice streams and may even become dominant in the grounding area, the shear stress as well as the longitudinal stress deviator are calculated in the whole two-dimensional ice sheet domain. Numerically, the ice sheet system model is solved on an irregular grid (both vertical and horizontal), which is fixed in space and time, with higher vertical resolution at the bottom of the ice sheet (where most of the shear takes place) and higher horizontal resolution in the grounding zone (to assure smooth grounding line migration). In this way, the model is capable of coping with the inhomogeneous and sometimes sparse distribution of ground truth in the Antarctic, thereby allowing detailed modeling in key areas. Moreover, detailed modeling in this way requires less computer time than in the case of fixed grid spacing.

A Cartesian co-ordinate system (x, z) with the x-axis parallel to the geoid and the z-axis pointing vertically upward ($z=0$ at sea level) is defined. Starting from the known bedrock topography and surface mass balance distribution, and assuming a constant ice density, the continuity equation for the ice thickness H then predicts the new ice thickness along the flow line:

$$\frac{\partial H}{\partial t} = -\frac{1}{b}\frac{\partial}{\partial x}(UHb) + M - S, \tag{1}$$

with U the depth averaged horizontal velocity [m a^{-1}], H the ice thickness [m], M the surface mass balance [m a^{-1}], and S the melting rate at the base of the ice sheet [m a^{-1}]. Divergence and convergence of the ice flow are taken into account in the calculation of the ice flux variation along the flow line through b [m], indicating the width of the flow band, and taken perpendicular to the flow line. Boundary conditions to the ice sheet system are zero surface gradients at the ice divide and a floating ice shelf at the seaward margin.

2.1. Velocity and stress field

An approximation often used in ice sheet modeling is that of plane flow, where all flow is supposed to take place in a vertical plane. Assuming furthermore that tractions at the upper surface are negligible, and that the ice sheet does not experience shear at its

sides ($\tau_{xy}=0$), the Stokes equations are often written as:

$$\frac{\partial \tau_{xz}}{\partial z} + 2\frac{\partial \tau'_{xx}}{\partial x} + \frac{\partial^2}{\partial x^2}\int_z^{H+h} \tau_{xz}\,dz = \rho g \frac{\partial (H+h)}{\partial x}, \tag{2}$$

where τ_{xz} is the shear stress, τ'_{xx} the longitudinal stress deviator, ρ the ice density (910 kg m^{-3}), g the acceleration due to gravity (9.81 m s^{-2}), and $z=h$ the elevation of the bottom of the ice sheet, so that $z=H+h$ coincides with the upper surface of the ice mass. The third term in the left hand side of eq. (2) is rather complex, involving the second derivative of the shear stress. This term (often called the T-term) accounts for bridging effects in the ice sheet and plays a role in the vicinity of the ice divide and at the grounding line. However, in most applications, this term is small and may be omitted from the force-budget calculations (HUTTER, 1983; VAN DER VEEN and WHILLANS, 1989). In order to find an expression for the shear stress, through vertical integration of eq. (2), a new vertical co-ordinate ζ, scaled to the local ice thickness, is introduced. This stretched dimensionless vertical co-ordinate is defined by $\zeta=(H+h-z)/H$, such that $\zeta=0$ at the ice surface and $\zeta=1$ at the base of the ice sheet (JENSSEN, 1977). Following the analysis of HUYBRECHTS and OERLEMANS (1988), the vertical domain was subdivided into 10 layers, with varying thickness, the upper layer thickness being $\Delta\zeta=0.15$ and with $\Delta\zeta=0.02$ near the bottom, where most of the shear and deformational heating take place. Introducing the scaled vertical co-ordinate, integrating eq. (2) with respect to ζ, and making use of the Leibnitz rule to change the order of integration, results in an expression for the shear stress :

$$\tau_{xz}(\zeta) = -\rho g H \zeta \frac{\partial (H+h)}{\partial x} - 2\frac{\partial}{\partial x}\left[H\int_\zeta^0 \tau'_{xx}(\zeta)\,d\zeta\right]$$

$$+2\tau'_{xx}(\zeta)\left[\frac{\partial (H+h)}{\partial x} - \zeta\frac{\partial H}{\partial x}\right]. \tag{3}$$

The model applies the generalized ice flow law. It is assumed that a Glen-type power relationship holds, with exponent $n=3$ (PATERSON, 1981). By invoking this constitutive relation the velocity field (in terms of velocity gradients) is related to the stress field. Since $\tau_{xz} = \tau'_{xz}$ and assuming that $\partial w/\partial x \ll \partial u/\partial z$, where w is the vertical and u is the horizontal velocity [m a^{-1}], this results in:

$$\dot{\varepsilon}_{xx} = \frac{\partial u}{\partial x}\Big|_z = \frac{\partial u}{\partial x}\Big|_\zeta + \frac{1}{H}\frac{\partial u}{\partial \zeta}\left[\frac{\partial (H+h)}{\partial x} - \zeta\frac{\partial H}{\partial x}\right] = A(T^*)(\tau'^2_{xx}+\tau^2_{xz})\tau'_{xx}, \tag{4a}$$

$$2\dot{\varepsilon}_{xz} = \frac{\partial u}{\partial z} = -\frac{1}{H}\frac{\partial u}{\partial \zeta} = 2A(T^*)(\tau'^2_{xx}+\tau^2_{xz})\tau'_{xz}, \tag{4b}$$

with $\dot{\varepsilon}_{ij}$ the strain-rate, which is related by definition to the velocity gradients (second term), and τ'_{ij} the stress components. The flow law parameter $A(T^*)$ is a function of

temperature T^* [K] (corrected for the dependence of the melting point on pressure: $T^* = T + 8.7\,10^{-4} H$) and several other parameters as well (crystal ice fabric, impurity contents,···). An Arrhenius relationship is adopted for $A(T^*)$ (see PATERSON, 1981; HUYBRECHTS and OERLEMANS, 1988).

Equation (3) contains the longitudinal stress deviator as unknown. An iterative numerical procedure is necessary to obtain τ'_{xx} from eq. (4a); it will be explained in Section 2.3. An expression for the horizontal velocity field is obtained by integrating eq. (4b) from the bottom of the ice sheet to an elevation ζ.

The basal sliding velocity $u(1)$ enters the velocity field as the lower boundary condition, but is only invoked when the base of the ice sheet reaches the pressure melting point. Following VAN DER VEEN (1987), who discusses different parameterizations of basal sliding, a Budd-sliding type is used:

$$u(1) = A_s \frac{\tau_d}{Z^{*2}}, \tag{5}$$

with $A_s = 75\ \mathrm{N^{-1}a^{-1}m^5}$, τ_d the driving stress $[-\rho g H \Delta(H+h)]$, and Z^* the height above buoyancy, defined as:

$$Z^* = H + \frac{\rho_w}{\rho}(h - H_{sl}). \tag{6}$$

Here ρ_w is the density of the sea water [1028 kg $\mathrm{m^{-3}}$] and H_{sl} the sea level stand with respect to the present conditions. With this relationship the basal friction is reduced in the area of the grounding line where the bottom of the ice sheet lies well below sea level and sea water infiltrates into the basal ice sheet layers, thus leading to higher sliding velocities. Since the continuity eq. (1) requires mass fluxes to be related to the rate of ice thickness change, a second integration of the velocity field from the bottom of the ice sheet to the surface yields the mean horizontal ice mass flux (UH). The vertical motion as a result of accumulation at the surface and vertical strain is calculated from the incompressibility condition and yields:

$$w(\zeta) = \int_0^{\zeta} \left[H \frac{\partial u}{\partial x}\Big|_{\zeta} + \frac{\partial u}{\partial \zeta}\left(\frac{\partial (H+h)}{\partial x} + \zeta \frac{\partial H}{\partial x} \right) \right] \mathrm{d}\zeta + w(0). \tag{7}$$

At the seaward margin of the ice sheet a freely floating ice shelf is coupled and the grounding line is simply determined by the flotation criterion. In contrast with the grounded ice sheet, the shear stress term in eq. (2) is omitted. In order to calculate the longitudinal deviatoric stress from this equilibrium, its value at the seaward edge of the shelf must be known. Here, the total force of the ice must be balanced by the sea water pressure, so that (THOMAS, 1973):

$$\tau'_{xx}(e) = \overline{\tau'_{xx}}(e) = \frac{1}{4} \rho g H \left(1 - \frac{\rho}{\rho_w} \right). \tag{8}$$

Using this expression to calculate the longitudinal stress deviator at the edge of the ice shelf, eq. (2) with the shear stress term set to zero is then integrated upstream to

yield the longitudinal deviatoric stress in the whole ice shelf. Once the vertical mean horizontal velocity at the grounding line is known, the integration with respect to x of eq. (4a) results in the ice shelf velocity field.

2.2. Temperature field and bed adjustment

The temperature distribution in an ice sheet is governed both by diffusion and advection, and is therefore dependent not only on boundary conditions such as surface temperature and geothermal heat flux, but also on ice velocity. The thermodynamic equation can thus be written as (HUYBRECHTS and OERLEMANS, 1988; RITZ, 1989):

$$\frac{\partial T}{\partial t} = \frac{k_i}{\rho c_p H^2}\frac{\partial^2 T}{\partial \zeta^2} - u(\zeta)\frac{\partial T}{\partial t}\Big|_\zeta$$

$$-\frac{1}{H}\frac{\partial T}{\partial \zeta}\left\{\frac{\partial (H+h)}{\partial t} + u(\zeta)\frac{\partial (H+h)}{\partial x} - \zeta\left[\frac{\partial H}{\partial t} + u(\zeta)\frac{\partial H}{\partial x}\right] - w(\zeta)\right\}$$

$$-\frac{1}{\rho c_p H}\frac{\partial u}{\partial \zeta}\tau_{xz}(\zeta), \qquad (9)$$

with T temperature [K], and k_i and c_p the thermal conductivity [J m^{-1}K^{-1}a^{-1}] and the specific heat capacity [J kg^{-1}K^{-1}] respectively. The heat transfer, as defined in eq. (9), is a result of vertical diffusion (first term), horizontal and vertical advection (second term and major part of the third term), and internal deformational heating caused by horizontal shear strain-rates (last term). Boundary conditions follow from the annual mean air temperature at the surface, and the geothermal heat flux (enhanced with heat from sliding friction) at the base (RITZ, 1987):

$$\left[\frac{\partial T}{\partial \zeta}\right]_{\zeta=1} = \frac{H}{k_i}\left[\rho g H \frac{\partial (H+h)}{\partial x} u(1) - \gamma_g\right], \qquad (10)$$

where γ_g [K m^{-1}] is the geothermal heat entering the ice at the base and written as a temperature gradient (RITZ, 1987, 1989). In order to calculate geothermal heating at the ice sheet base the thermal conductivity in the underlying bedrock is also taken into account. As shown by RITZ (1987) and HUYBRECHTS (1992), this effect may seriously damp the basal temperature response for climatic oscillations operating on longer time scales. For the calculation of the heat transfer in the underlying bed, only vertical diffusion needs to be taken into account. Following HUYBRECHTS (1992) a rock slab of 2000 m thickness is considered, divided into 5 equally spaced layers. In most experiments geothermal heating was treated as a constant $\gamma_g = G/k_i$, with G the geothermal heat flux entering the base of the ice sheet. A nominal value for G of 54.4 mW m^{-2} or 1.72 10^6 J m^{-2} a^{-1} was taken (SCLATER *et al.*, 1980), which corresponds to 1.30 HFU (Heat Flow Units; 1 HFU = 41.48 mW m^{-2}).

The basal temperature in the ice sheet is kept at the pressure-dependent melting point whenever it is reached, and the surplus energy is used for melting. This may, in

some cases, lead to the formation of a temperate ice layer between $\zeta=1$ and $\zeta=\zeta_{\text{melt}}$, so that the basal melt rate S is defined as:

$$S=\frac{k_i}{\rho H L}\left[\left(\frac{\partial T}{\partial \zeta}\right)_b-\left(\frac{\partial T}{\partial \zeta}\right)_c\right]+\frac{1}{\rho L}\int_1^{\zeta_{\text{melt}}}\frac{\partial u}{\partial \zeta}\tau_{xz}(\zeta)\,\mathrm{d}\zeta, \tag{11}$$

where indexes b and c denote the basal temperature gradient as given in eq. (10) and the basal temperature gradient after correction for pressure melting respectively, and L the latent heat of fusion [3.35 10^5 J kg^{-1}]. In the ice shelf, the vertical temperature profile is taken to vary linearly with the surface temperature as the upper boundary condition and a constant temperature of -2°C at the bottom of the ice shelf. Melting or refreezing processes at the ice-sea water contact are not taken into account.

Bed adjustments are calculated in a very simplified way, only by considering the isostatic changes locally. The time dependent response is modeled by a diffusion equation for bedrock elevation h_b, as described in HUYBRECHTS (1992).

2.3. Numerical calculation

The two-dimensional ice sheet system model is implemented on a flow line the domain of which extends from the ice divide to the edge of the continental shelf. Because of the non-linear nature of the velocity in the ice sheet, the continuity eq. (1) is reformulated as a non-linear partial differential equation and written as:

$$\frac{\partial H}{\partial t}=\frac{1}{b(x)}\frac{\partial}{\partial x}\left[b(x)D(x)\frac{\partial(H+h)}{\partial x}\right]+M-S, \tag{12}$$

with $D(x)$ a diffusion coefficient which, in the grounded ice sheet, equals the mass flux (UH) divided by the surface gradient. Note however that the diffusion coefficient in eq. (12) is taken positive in the direction of the flow. A solution to this equation can be obtained by writing eq. (12) in the conservation form (MITCHELL and GRIFFITHS, 1980). For the numerical computation a semi-implicit scheme was applied, and new ice thicknesses on the next time step were found by the solution of a tridiagonal system of equations. An implicit numerical scheme was adopted for the ice and rock temperature field, resulting in a similar set of tridiagonal equations.

The longitudinal stress deviator in the ice sheet is obtained by a numerical root finding method, and eq. (4a) is therefore rewritten as a function $f(y=\tau'_{xx})=0$. An efficient algorithm for one-dimensional root finding is the Newton-Raphson method using the derivative (or a hybrid algorithm that takes a bisection step whenever Newton-Raphson would take a solution out of bounds). However, in some cases, Newton-Raphson fails and Laguerre's method, a general complex root finding algorithm, was applied (PRESS *et al.*, 1992).

The numerical solution for the horizontal velocity in the ice sheet as well as in the ice shelf is also performed iteratively: (i) calculate the two-dimensional shear stress using eq. (3); (ii) determine the horizontal velocity field in the ice sheet; (iii) calculate the longitudinal stress deviator and the velocity field in the ice shelf; (iv) using the above described root finding method, calculate the longitudinal deviator stress in the ice sheet

from eq. (4a); (v) repeat steps (i) through (iv) until the velocity field attains a stable solution. Normally, no more than two of these giant iteration steps are necessary.

3. Model Input and Forcing Parameters

The primary input for the model is the bedrock and ice surface profile sampled along the central flow line of Shirase Drainage Basin from the ice divide (Dome F) to the edge of the continental shelf. Data were sampled from the oversnow traverses from Syowa Station to Dome F during the 1992 field season (KAMIYAMA *et al.*, 1994) and smaller traverses in the area (WATANABE *et al.*, 1992). Detailed subglacial reference in the stream region was compiled after MAE and YOSHIDA (1987) and in the ice shelf area after MORIWAKI and YOSHIDA (1983). These data were sampled with an approximate grid size of 20 km, decreasing to 10 km in the grounding area, leading to a flow line of about 1100 km in length. Convergence and divergence of the ice flow was digitized from the topographic map of the region (AGETA *et al.*, 1995) by drawing two flow lines at each side of the central flow line and measuring in each grid point the flow band width (b) perpendicular to the central line.

From 79 measurements of 10 m snow depth temperatures (SATOW and KUKUCHI, 1995) ranging from an elevation of 250 m to 3760 m a.s.l. in Shirase Drainage Basin, surface temperature was parameterized both as a function of surface elevation and latitude, thereby following FORTUIN and OERLEMANS (1990):

$$T_s = B_1 (H+h) + B_2 \phi + B_3 + \Delta T, \tag{13}$$

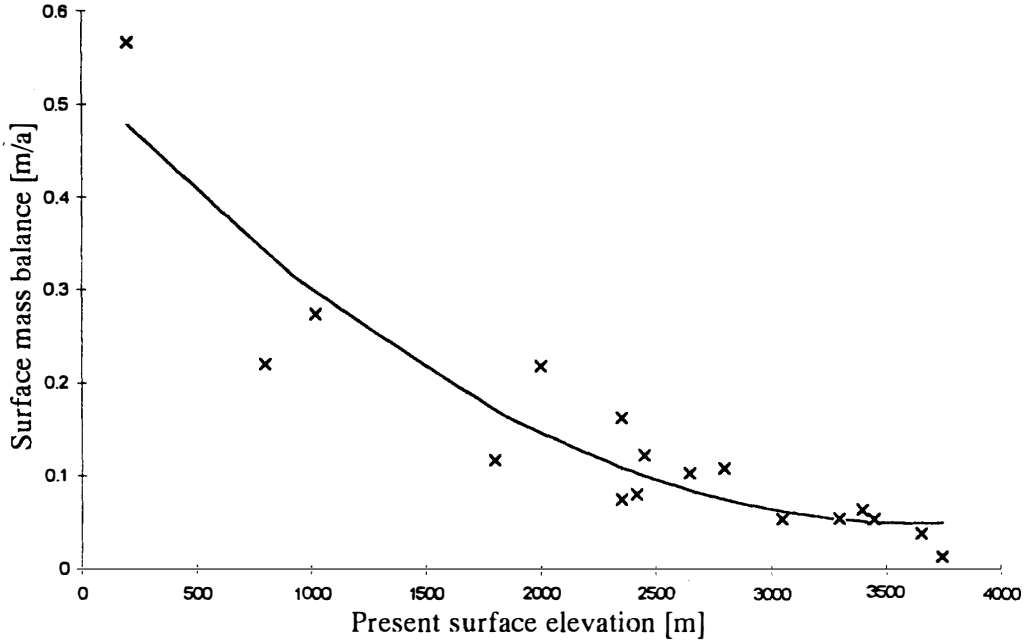

Fig. 2. Mass balance measurements derived from snow pit measurements in Shirase Drainage Basin (TAKAHASHI and WATANABE, 1995), and the parameterization of the surface mass balance as a function of the present surface elevation in order to obtain a continuous record of the present mass balance distribution along the flow line.

where $B_1 = -0.01085$, $B_2 = -0.222244$, $B_3 = 6.440234$ for a surface elevation lower than 2000 m a.s.l. and $B_1 = -0.011068$, $B_2 = -0.820738$, $B_3 = 48.623326$ otherwise. In eq. (13) the surface temperature T_s and latitude ϕ are expressed in °C and in degrees south respectively, and ΔT is the background temperature forcing applied at sea level in the climatic forcing experiments ($\Delta T = 0$ at present). The mean annual surface mass balance was parameterized from snow pit observations measured by the gross β-profile method (TAKAHASHI and WATANABE, 1995). A second degree polynomial as a function of *present* surface elevation was adopted in order to obtain a continuous record of present mass balance distribution along the flow line (Fig. 2):

$$M(0) = 0.529 - 2.63\ 10^{-4}\,(H+h)_0 + 3.612\ 10^{-8}\,(H+h)_0^2, \qquad (14)$$

where $M(0)$ is the present mass balance [m a^{-1} ice equivalent]. At the coast the present mass balance equals approximately 0.5 m a^{-1}, while at the ice divide (3700–4000 m) the present mass balance is around 0.05 m a^{-1}, which is in accord with the measurements in Shirase Drainage Basin and parameterizations over the East Antarctic ice sheet.

Although we ignore at present the precise environmental conditions reigning in Shirase Drainage Basin during the last glacial maximum and beyond, the proximity to the central ice divide suggests the use of climatic forcing similar to that found for the Vostok ice core. Drilling experiments are at present being carried out at Dome F and the climatic record will only be available in a few years. As explained above, during the experiments surface temperature is perturbed by changes in background temperature ΔT (assumed uniform over the ice sheet) and by local changes in surface elevation. Changes in surface temperature also affect accumulation rates in different climates. Following LORIUS *et al.* (1985) the accumulation rate $M(t)$ in the past is calculated from its present value $M(0)$ time the ratio of the derivatives of the saturation vapor pressure with respect to $T_f(t)$ and with respect to $T_f(0)$, where T_f is the temperature above the inversion layer:

$$M(t) = M(0) \exp\left[22.47\left(\frac{T_0}{T_f(0)} - \frac{T_0}{T_f(t)}\right)\right]\left[\frac{T_f(0)}{T_f(t)}\right]^2. \qquad (15)$$

To relate the temperature above the inversion layer (T_f) to the surface temperature (T_s) the relation proposed by JOUZEL and MERLIVAT (1984) was used: $T_f(t) = 0.67\ T_s(t) + 88.9$, where $T_s(t)$ is the surface temperature [K] and $T_0 = 273.15$ K (see also HUYBRECHTS, 1990). Applying this formula for a temperature decrease of 10°C during the last glacial maximum we find for each point of the glacier profile (assuming that the temperature decreases with altitude) an accumulation rate which is roughly 50–60% of the present one.

4. Steady State Experiments

The purpose of the steady state experiments with the ice sheet system model is twofold: (i) to adjust the model to the present height-to-width ratio (tuning purposes), and (ii) to examine the local ice sheet characteristics, such as ice thickness distribution, surface and basal velocities, which are compared to the present observed values. Starting

from the present bedrock and surface topography of Shirase Drainage Basin, the present mass balance and temperature distribution, the model ran forward in time to calculate the two-dimensional temperature field, with the ice thickness not allowed to change in time (temperature initialization). In a second run the temperature and velocity flow field were coupled through the Arrhenius relationship and ice thickness was allowed to respond, until a steady state was reached after about 200 ka. These large response time scales are due to slow temperature re-distribution in the central ice sheet, caused by the

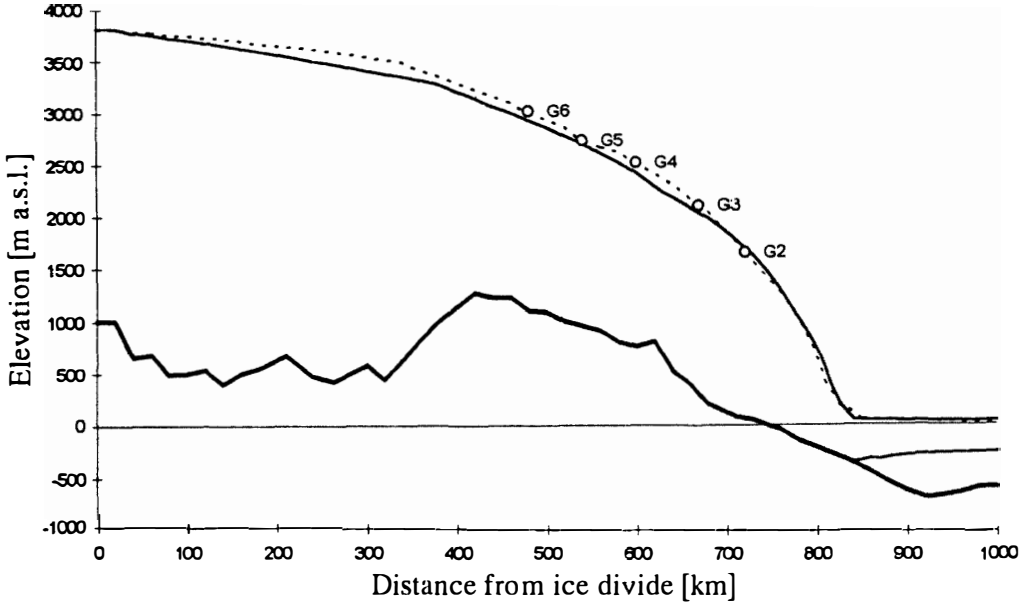

Fig. 3. Present observed (dashed line) and steady state modeled (solid line) surface profile of Shirase Glacier from dome F (ice divide) to Lützow-Holm Bay. Stations G2 to G6 are also displayed as a reference.

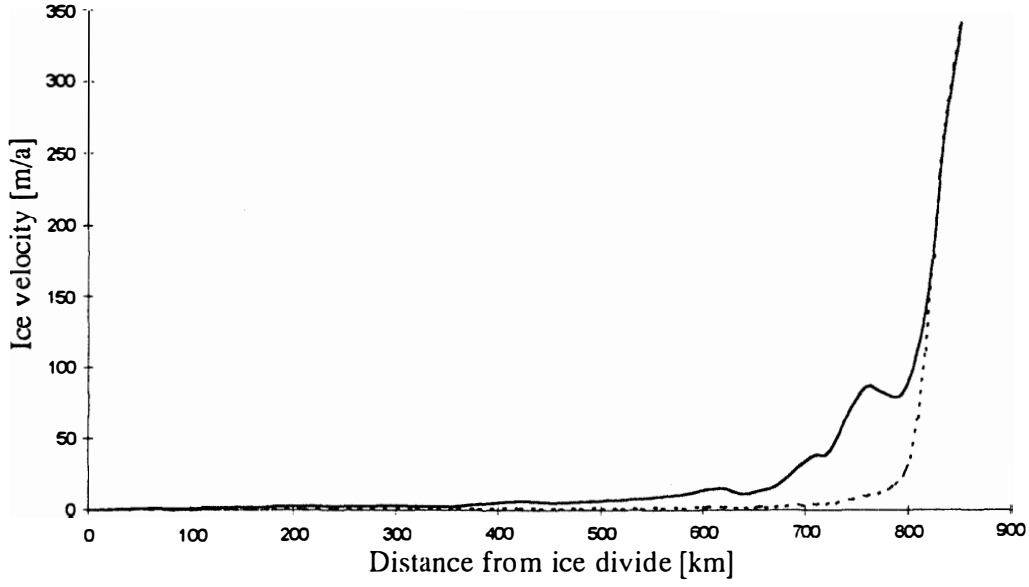

Fig. 4. modeled surface (solid line) and basal (dashed line) ice velocities from the ice divide to the grounding line in the steady state ice sheet configuration.

Table 1. Comparison of measured horizontal surface velocity different stations on Mizuho Plateau with present steady state modeled values. Also listed are the modeled basal siding velocity and the basal shear stress.

Station	$u(H+h)$ [m/a] measured	$u(H+h)$ [m/a] model	$u(h)$ [m/a] model	τ_b [Pa] model
G6	8*	6	0.6	58811
G5	13*	8	0.8	66072
G4	20*	14	1.3	83830
G3	29*	17	1.9	82388
G2	36*	39	3.8	110549
gr. line	2000–2500**	253	251.8	40047

Source : *NISHIO *et al.* (1989), **FUJII (1981).

relatively small advection rates. A close fit between the present observed and the modeled surface profile was obtained by multiplying $A(T^*)$ by values of 0.6 and 0.1 for the ice sheet and the ice shelf respectively (Fig. 3): the ice thickness distribution along the flow line corresponds within 150 m with the present observed values. These so-called 'tuning' values were adopted for all further modeling experiments, and they implicitly deal with softening effects caused by impurity content and crystal fabric (PATERSON, 1981; HUYBRECHTS, 1992). Horizontal surface velocities are in overall agreement with the observed values at Mizuho Plateau (Fig. 4 and Table 1). However, in the stream region of Shirase Glacier (grounding line) horizontal surface velocities are one order of magnitude lower than the observed values. Obviously, the large convergence of the ice flow is not sufficient to cause a large increase in the downstream surface velocity (from 40 ma^{-1} at Mizuho Plateau to 2500 ma^{-1} in the ice stream). Some other flow mechanism should probably account for this. If the ice is not frozen to the bed and basal conditions are such that the sliding velocity and its downstream gradient are small—as is the case at Mizuho Plateau—longitudinal strain-rate or stretching may be neglected relative to the shear strain-rate and movement will be mostly by shearing only. However, as the sliding velocity increases, its down-stream gradient (which is equal to the longitudinal strain-rate) may become comparable in magnitude to the shear strain-rate and stretching may no longer be negligible compared with shearing. In case of a surging glacier, for example, the sliding velocity is so large that stretching becomes the dominant deformation process (MCMEEKING and JOHNSON, 1985). The present model description properly takes account of these features of the ice dynamics at the grounding line by including longitudinal stresses, which in case of increased basal sliding become the major stress contributor in this area. A limiting factor, however, remains the basal sliding velocity, which enters the velocity field as the lower boundary condition, and its parameterization remains a crude approximation (as a function of local ice sheet geometry) which might not take full account of the real basal stream mechanics. A possible solution can be found in treating the ice stream dynamics as a 'shelfy stream' (MUSZYNSKI and BIRCHFIELD, 1987; HINDMARSH, 1993), an ice stream with shelf-like mechanics. However, apart from some analytical models, the dynamics of ice streams remain not well understood.

Figure 5 displays the present modeled vertical profiles of the longitudinal deviatoric and shear stress at the grounding line and the longitudinal deviatoric stress at the first ice

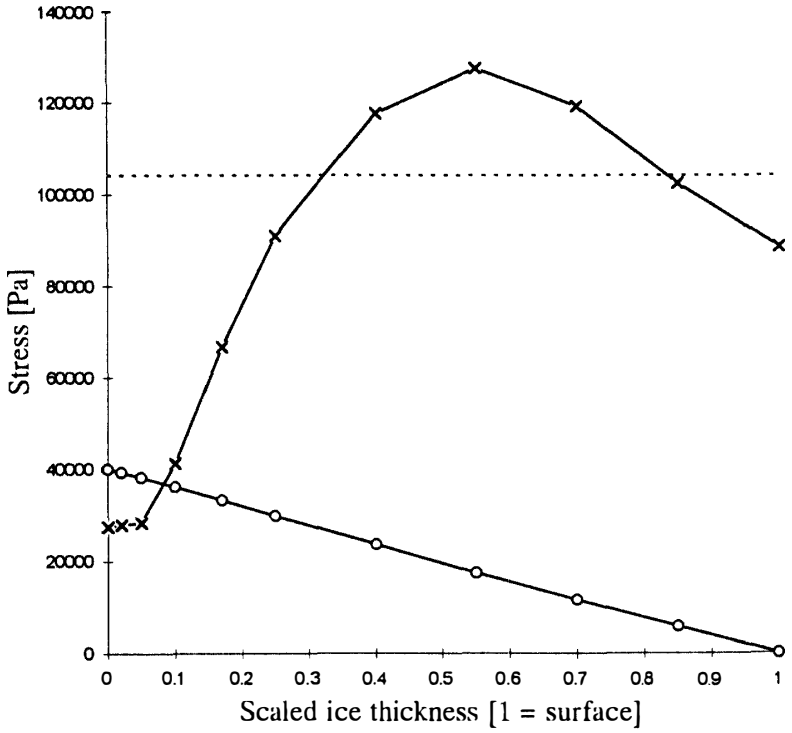

Fig. 5. Vertical profiles of the stress field at the grounding area in the steady state modeled ice sheet: shear stress at the grounding line (circles), longitudinal deviatoric stress at the grounding line (crosses) and longitudinal deviatoric stress at the first grid point of the ice shelf (dashed line).

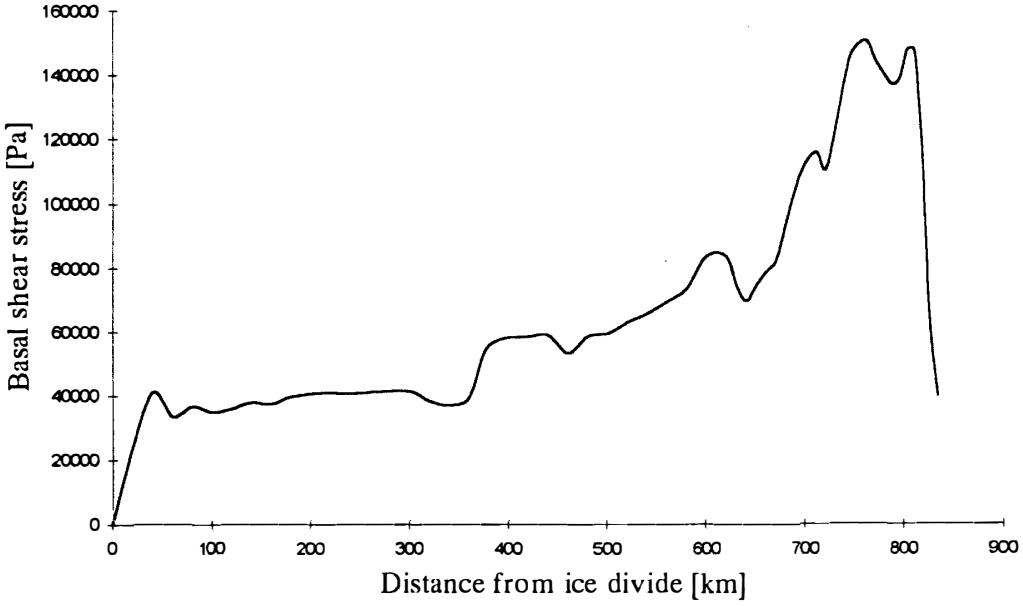

Fig. 6. Basal shear stress distribution along the flow line from the ice divide to the grounding line in the steady state ice sheet configuration.

shelf grid point (where the shear stress equals zero). At the grounding line, the longitudinal deviatoric stress dominates the shear stress and reaches locally even higher values than in the ice shelf. Nevertheless, the shear stress cannot be neglected and is even

larger than the longitudinal deviatoric stress at the base of the ice sheet.

Due to the basal sliding and longitudinal stretching in the transition zone between the ice sheet and the ice shelf the surface slope decreases. An immediate consequence of the decreasing downstream surface slope and ice thickness is that the basal shear stress will not reach its maximum at the ice sheet edge, but somewhat more upstream as shown in Fig. 6. Despite the conclusion of MAE (1979) that a similar profile of the basal shear stress along the central flow line should indicate that the ice sheet is not in steady state or that this profile resembles the profile of surging glaciers, Fig. 6 displays a steady state ice sheet solution.

In the standard model experiments carried out in this paper a constant value for the geothermal heat flux of 1.30 HFU (Heat Flow Units) was used. This means that the heat conduction in the bedrock was not calculated explicitly, thus allowing smaller response time scales. In order to investigate the sensitivity of the ice sheet to changes in the geothermal heat flux, two experiments were run with a geothermal heat flux of 1.24 (-5%) and 1.37 ($+5\%$) HFU respectively. Although an increase of 5% enlarges the area which is subject to pressure melting, the changes in surface elevation under steady state conditions are of the order of 20 m and thus are negligible. The same conclusion can be drawn when decreasing the geothermal heat flux by 5%. The smaller area where the temperature at the bottom of the ice sheet reaches the pressure melting point does not lead to substantial changes in ice thickness either.

5. Dynamic Sensitivity: Local Imbalance

In order to study the dynamic sensitivity of Shirase Drainage Basin and its present local imbalance (or thinning rate) the evolution of the ice sheet was simulated during a complete glacial-interglacial cycle. As an initial configuration, the model was run in a

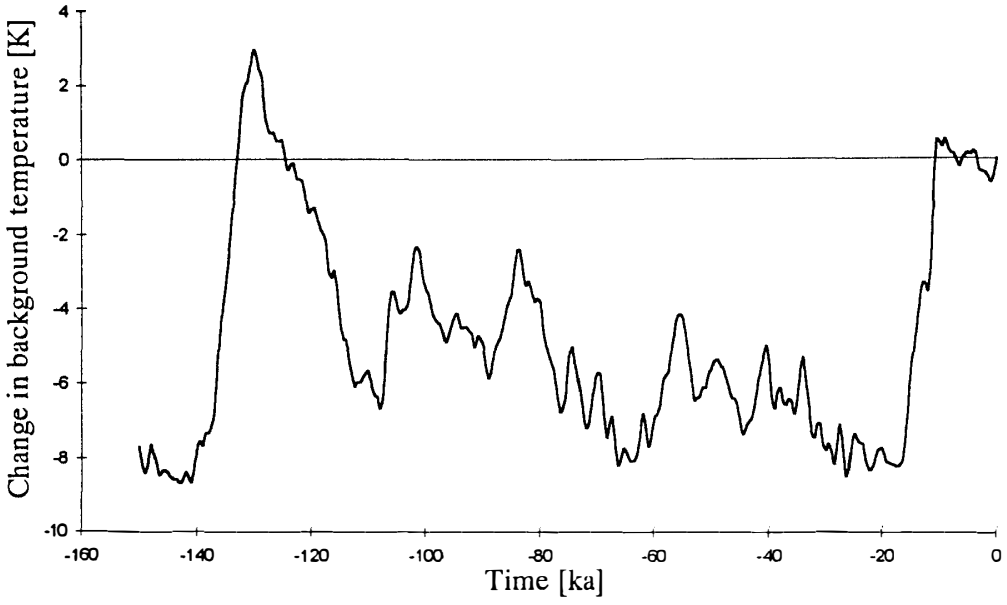

Fig. 7a. Vostok ice core temperature signal (JOUZEL et al., 1987) from 150 ka BP until present used as background forcing in the dynamic experiments. Data were sampled at a 100 year interval.

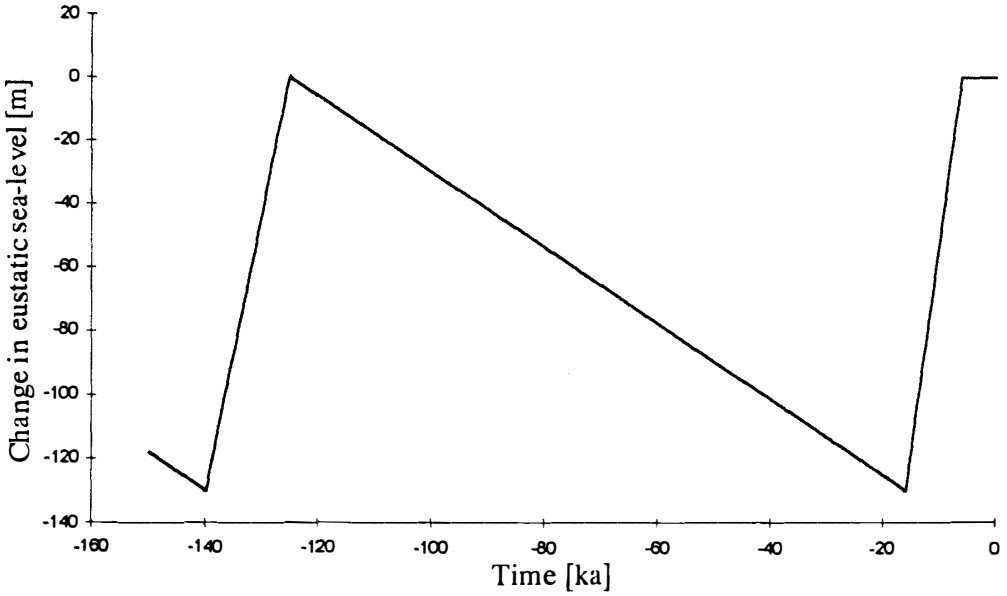

Fig. 7b. Adopted sea-level changes (HUYBRECHTS, 1992) from 150 ka BP until present used as background forcing in the dynamic experiments. Data were sampled at a 100 year interval.

steady state with a background temperature 8 °C lower than at present, which also reduces the mass balance distribution according to eq. (15), and with a sea-level lowering of 120 m, reflecting the environmental conditions reigning at 150 ka BP. Starting from this steady state situation, the ice sheet was run forward in time until present, forced by the Vostok ice core temperature signal (JOUZEL *et al.*, 1987) and by changes in the eustatic sea-level according to a sawtooth function (Figs. 7a and b). This latter function was adopted from HUYBRECHTS (1992) and taken as an intermediate between the oxygen isotope record from the deep Pacific and a sea-level record derived from a sequence of raised marine terraces in New Guinea, which are both discussed by CHAPPELL and SHACKLETON (1986) and SHACKLETON (1987).

Three glacial-interglacial experiments were performed: (i) the standard model run with a constant geothermal heat flux of 1.30 HFU, (ii) an experiment where the heat conduction in the bedrock was calculated and (iii) an experiment including local isostatic bedrock adjustment.

5.1. The Shirase Drainage Basin during a glacial-interglacial cycle

Figures 8a–c display the ice sheet surface elevation during the course of the glacial-interglacial cycle for the ice divide, stations G6 and G4 respectively. However, before starting a more detailed analysis of the elevation changes during the course of this glacial-interglacial cycle, it is helpful to recall the basic conclusions drawn from steady state experiments regarding the nature of the response of the ice sheet due to a sudden change of environmental parameters. Such basic sensitivity experiments have been carried out by PATTYN *et al.* (1989) with a flow line model applied to glaciers in the Sør Rondane, Dronning Maud Land and also by HUYBRECHTS (1990) with a three-dimensional model of the Antarctic ice sheet. In spite of large differences in complexity

between the two models, results of the sensitivity experiments in both studies give the same global picture. In PATTYN *et al.* (1989) the model was run in a steady state for different climatic scenarios: (i) a general lowering of the accumulation rate with 50%, (ii) a decrease in background temperature with 11 °C, (iii) a lowering of sea-level with

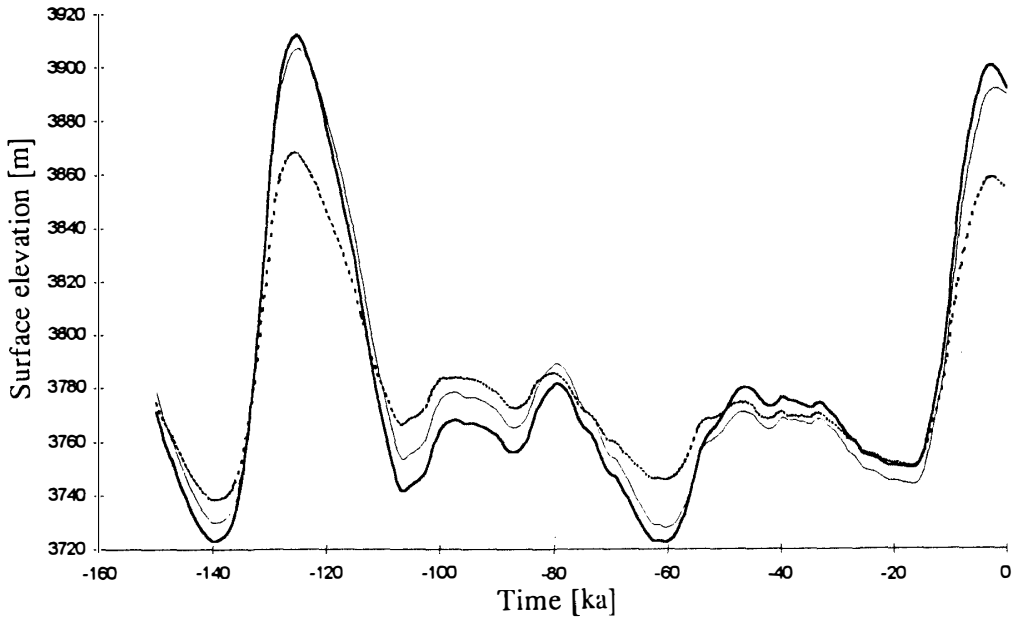

Fig. 8a. Local surface elevation changes at the ice divide when forcing the model with the temperature and sea-level signal as shown in Figs. 8a and b. The model run starts at 150 ka BP from a steady state situation with background temperature 8 °C lower and sea-level 120 m lower than present. Displayed are the standard experiment with a constant geothermal heat flux of 1.30 HFU (solid line), including heat conduction in the bedrock (thin solid line), and including local isostatic bedrock adjustment (dashed line).

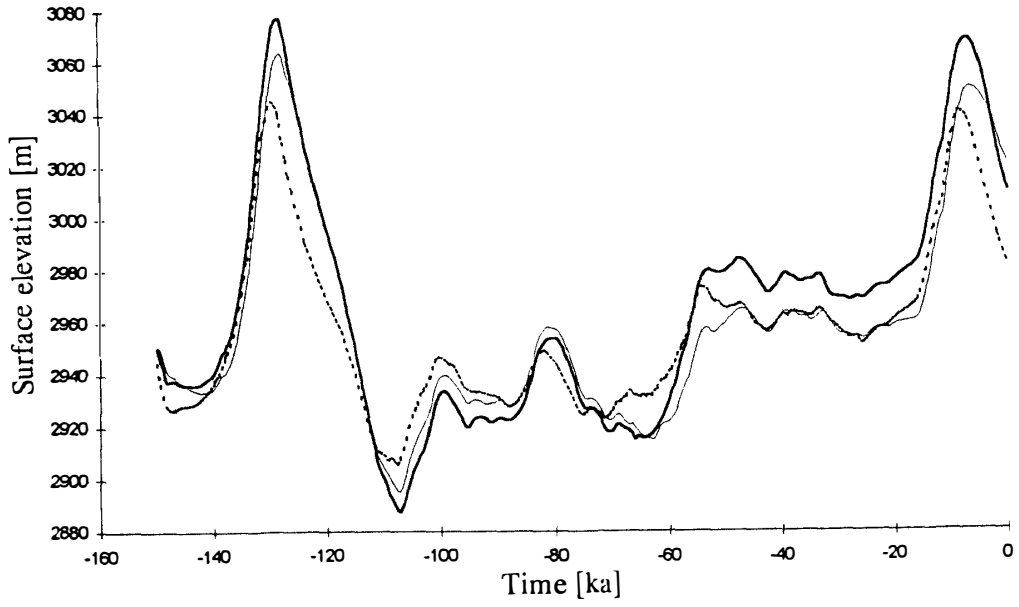

Fig. 8b. Same as Fig. 8a, but the corresponding surface elevation changes at station G6.

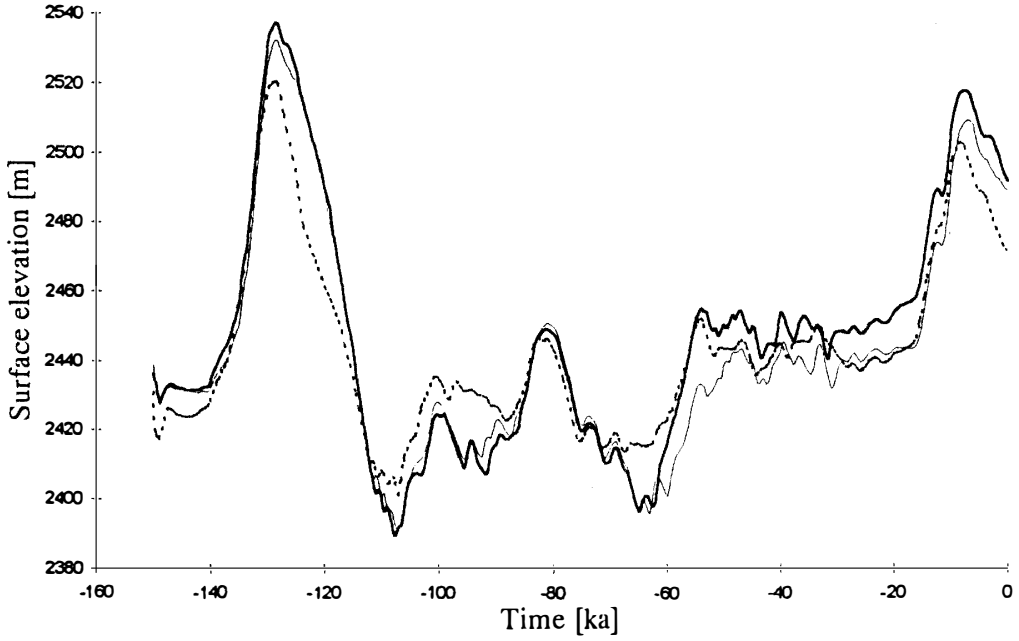

Fig. 8c. Same as Fig. 8a, but the corresponding surface elevation changes at station G4.

150 m, and several combinations of these elements. Results revealed that the most decisive single environmental parameter is a temperature drop of 11 °C, which stiffens the ice and consequently results in a buildup of ice. This effect is further enhanced by lowering sea-level, causing an additional seaward migration of the grounding line. Grounding line movements caused by sea-level lowering will only affect the coastal area and not the central ice sheet area, while colder temperatures affect the whole ice sheet. Colder climates are believed to be accompanied by reduced accumulation rates, so that the above mentioned ice sheet expansion due to stiffening of the ice will be compensated for by lower precipitation rates, hence resulting in a rather small surface elevation increase. It should be emphasized that these results relate to steady state conditions, and will consequently differ from the present dynamic experiments in which the environment is subject to a continuous change. Thus, from Figs. 8a–c the following conclusions can be drawn:

(i) The overall amplitude in surface elevation change due to a glacial-interglacial contrast measures 190 m at the inland part down to 150 m at G4. Maximum ice sheet elevation occurs for the three stations (divide, G6 and G4) approximately at the same time (125–130 ka BP and 5–10 ka BP), which more or less coincides with the penultimate and ultimate climatic optima respectively.

(ii) Surface elevation changes at the ice divide follow with a greater time lag than the elevation changes at Mizuho Plateau. For example, the maximum surface elevation near the divide at the beginning of the penultimate and ultimate interglacials is reached approximately 4000 years later than at station G4. This larger response time is probably due to thermo-mechanical effects: a change in surface temperature will reach the basal ice sheet layers more rapidly when advection rates are relatively high, such as is the case at Mizuho Plateau, thus influencing the ice sheet flow characteristics. Thus, ice thickness and basal stresses near the ice divide need much more time to adapt to a changing mass

balance field, due to the low advection rates.

(iii) Between the two interglacial periods, the ice sheet surface is relatively low due to the lower precipitation rates. The surface elevation changes clearly follow the mass balance perturbation, which is similar to the course of the temperature curve. Stiffening of the ice seems to have only a small effect. The full effect of the ice stiffening obviously needs larger time scales than a glacial-interglacial cycle, *i.e.* at the glacial maximum the basal temperature is not as low as is the case when running the model into a steady state under similar environmental conditions. During the glacial period, a gradual ice buildup can be observed at stations G6 and G4, in which the sea-level lowering and associated seaward grounding line migration play a decisive role. As mentioned earlier, the grounding line migration has no effect on the surface elevation changes at the divide.

(iv) During the last glacial maximum the ice sheet reached its maximum lateral expansion, due to the low sea-level (−130 m compared to present). The combined effect with the low precipitation rates resulted in an overall surface elevation which was much lower than observed at present.

(v) The sudden increase in precipitation due to a temperature shift between the last glacial maximum and the Holocene finally resulted in a maximum surface elevation at the beginning of the last interglacial, even though at the same time the ice sheet shrinks in length due to the associated sea-level rise. At present, the ice sheet surface is still lowering at approximately the same rate as around 120 ka BP.

A closer look at the proper curves reveals that there is almost no difference in ice sheet response when including heat conduction in the bedrock or not (constant geothermal heat flux of 1.30 HFU). Nevertheless, the amplitude of the basal temperature change at station G4 (Fig. 9) is almost twice as large in the standard experiment as compared to the experiment including heat conduction in the bedrock. This discrepancy is due to the damping effect of the thermal conductivity in rock on the basal tempera-

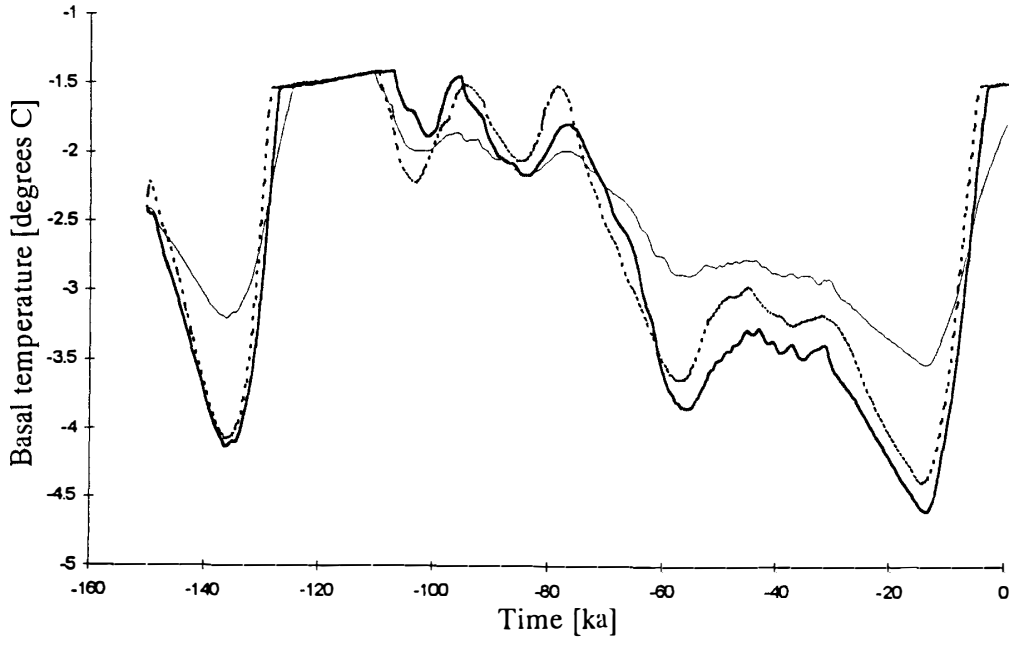

Fig. 9. Basal temperature variations at station G4 corresponding to the experiments described in Fig. 8.

tures response (RITZ, 1987). On the other hand, including bedrock adjustment seriously reduces the amplitude in ice sheet response on the glacial-interglacial scale, since larger ice thickness forces the bedrock to sink, hence resulting in a lowering of the ice sheet surface.

5.2. Present local imbalance

The regional variation of the present local imbalance along the flow line (Fig. 10 and Table 2) is calculated as the mean imbalance over the last 1000 years. The largest

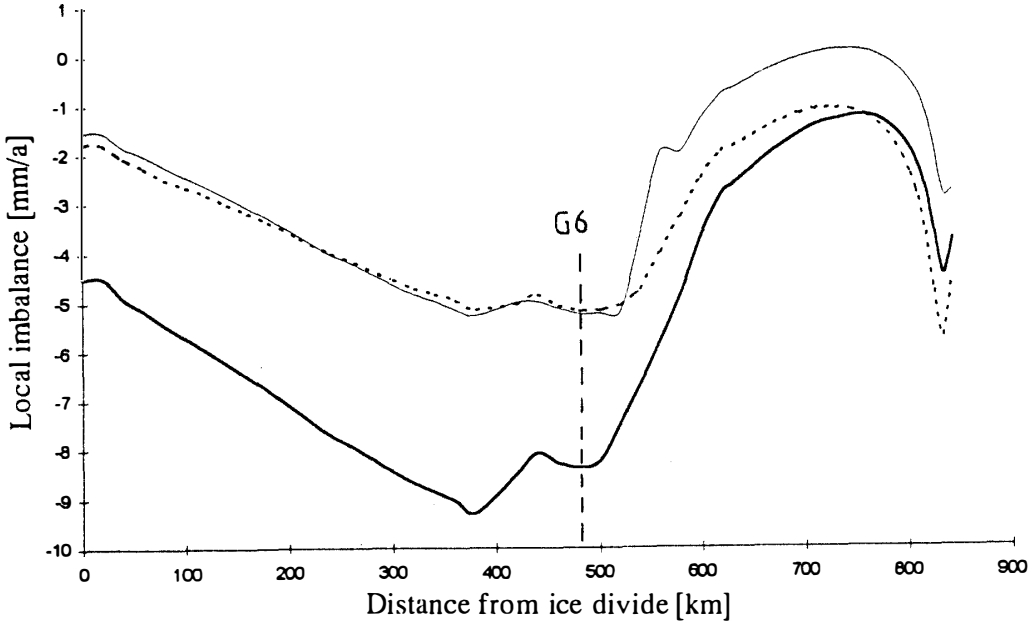

Fig. 10. Present local imbalance along the flow line from the ice divide to the grounding line, calculated as the mean imbalance over the last 1000 years. Displayed are the standard experiment with a constant geothermal heat flux of 1.30 HFU (solid line), including heat conduction in the bedrock (thin solid line), and including local isostatic bedrock adjustment (dashed line).

Table 2. Comparison of the measured thinning rate (local imbalance [mm/a]) for different stations on Mizuho Plateau (in snow depth) and model calculations (in ice depth) after forcing with the Vostok temperature signal. Model 1=standard model run with constant geothermal heat flux set at 1.30 HFU; Model 2=with heat conduction in the bedrock; Model 3=with bedrock adjustment.

Station	$\partial(H+h)/\partial t$ measured	$\partial(H+h)/\partial t$ model 1	$\partial(H+h)/\partial t$ model 2	$\partial(H+h)/\partial t$ model 3
Ice divide	–	−4.5	−1.5	−1.8
G6	−400*	−8.4	−5.2	−5.2
G5	−400*	−6.7	−3.7	−4.7
G4	−1200*	−3.6	−1.3	−2.5
G3	−2300*	−1.9	−0.2	−1.4
G2	−3100*	−1.3	+0.1	−1.1
gr. line	–	−3.7	−2.8	−4.5

Source : *NISHIO *et al.* (1989).

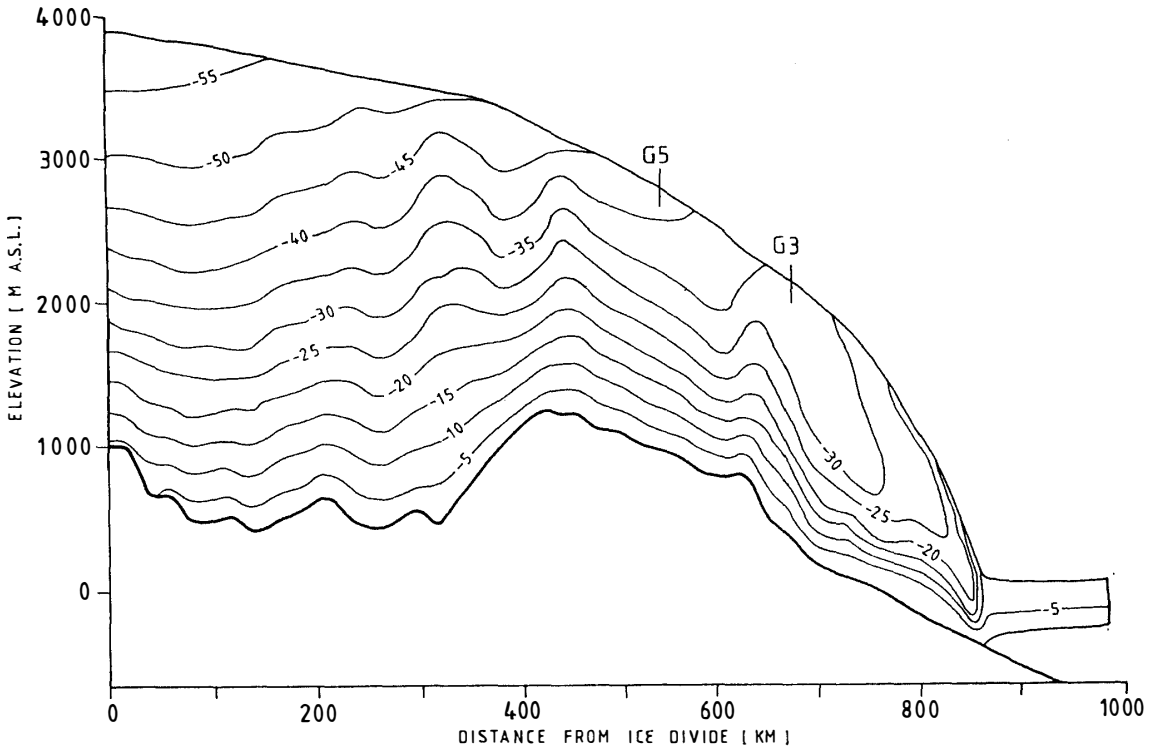

Fig. 11. Present modeled temperature distribution in the ice sheet after 150 ka of integration, corresponding to the standard experiment.

imbalance is found south of station G6, with a thinning of 9 mm a^{-1} according to the standard model run. Including bedrock adjustment or heat conduction in the bedrock accounts for smaller thinning rates in both cases.

Finally, the present temperature distribution in the ice sheet after 150 ka of integration is given in Fig. 11. A large part of the ice sheet base is subject to pressure melting. This is a larger area than is presumed at present by calculating the temperature profile based on a simple steady state model of heat conduction (NISHIO *et al.*, 1989). Also, between G3 and G5 our model points to warmer ice in the upper layers compared to the steady state model, due to the rather slow horizontal advection of cold ice toward the stream area.

6. Discussion and Conclusion

The present ice sheet system model is an improvement compared to previous ice sheet modeling experiments and is capable of explaining the major characteristics of the Shirase Drainage Basin. Field data and model output over the central ice sheet area and Mizuho Plateau are in overall accordance. However, the model reveals that the ice dynamics at the grounding area, or stream region, probably differs from the presently assumed dynamics at the grounding line (for instance in the way longitudinal stresses are included). Apart from a few horizontal surface velocities (FUJII, 1981) little is known in this drainage key area. Boundary conditions at the base remain the biggest factor of uncertainty, especially the way in which the basal sliding, entering the velocity

field as a boundary condition, is parameterized.

Sensitivity experiments showed that the inclusion of bedrock heat conduction did not alter the overall ice sheet behavior significantly, nor did small variations in the geothermal heat flux. Bedrock adjustment, on the other hand, seemed to be a more decisive factor.

By simulating the Shirase Drainage Basin during the course of a complete glacial-interglacial cycle the transient behavior of the ice sheet could be explained as well as the present local imbalance as a result of past climatic changes. The modeled imbalance values, which are more or less in accord with the values obtained from a similar kind of experiment described by HUYBRECHTS (1992) for the Antarctic ice sheet as a whole, point to an overall thinning of the ice sheet of 5–10 mm a^{-1}. The present observed thinning rates in Shirase Drainage Basin are, however, much larger (100–1000 mm a^{-1}). From the fact that during interglacial periods (such as as present) the pressure melting point is reached at the base of the ice sheet in Mizuho Plateau and further downstream, basal sliding seems a natural process to occur and not an event which has recently started. Even under these conditions the ice sheet system model is capable of producing a stable steady state solution in which the modeled surface topography hardly deviates from the present observed situation. However, as the model is not capable of simulating the high surface velocities presently observed in Shirase Glacier, it seems more acceptable to assume that possible changes in the dynamics of the stream area and the ice shelf/ice tongue could be responsible for the considerable recent ice variations in Shirase Drainage Basin, as observed in the field. This opinion is further confirmed by the fact that major thinning is observed in the downstream area and gradually decreases upstream. Further modeling experiments will therefore be focused on the ice dynamics in the stream area.

Acknowledgements

This paper forms a contribution to the Belgian Scientific Research Program on Antarctica (Science Policy Office), contract A3/03/002. The authors are deeply indebted to Prof. O. WATANABE and Prof. Y. FUJII of the National Institute of Polar Research (NIPR), Tokyo, Japan for helpful discussions on the dynamics of Shirase Glacier and for supplying all data necessary for carrying out this study. We thank also Prof. R. NARUSE and an anonymous referee for adding valuable comments.

References

AGETA, Y., NISHIO, F., FUJII, Y. and MORIWAKI, K. (1995): Ice sheet surface. Antarctica, East Queen Maud Land, Enderby Land; Glaciological Folio, ed. by A. HIGASHI. Tokyo, Natl Inst. Polar Res.

BINDSCHADLER, R. (1983): The importance of pressurized subglacial water in separation and sliding at the glacier bed. J. Glaciol., **29** (101), 3–19.

CHAPPELL, J. and SHACKLETON, N.J. (1986): Oxygen isotopes and sea level, Nature, **324**, 137–140.

DENTON, G.H., SUGDEN, D.E., MARCHANT, D.R., HALL, B.L. and WILCH, T.I. (1993): East Antarctic ice sheet sensitivity to Pliocene climatic change from a Dry Valleys perspective. Geogr. Ann., **75A** (4), 155–204.

FORTUIN, J.P.F. and OERLEMANS, J. (1990): Parameterization of the annual surface temperature and mass

balance of Antarctica. Ann. Glaciol., **14**, 78–84.

FUJII, Y. (1981): Aerophotographic interpretation of surface features and estimation of ice discharge at the outlet of the Shirase Drainage Basin, Antarctica. Nankyoku Shiryô (Antarct. Rec.), **72**, 1–15.

FUJITA, S., IKEDA, N., AZUMA, N., HONDOH, T. and MAE, S. (1991): Numerical estimation of 104 years later equilibrium ice sheet profile in the Shirase Glacier Drainage Basin, East Antarctica. Nankyoku Shiryô (Antarct. Rec.), **35**, 12–29.

HINDMARSH, R.C.A. (1993): Qualitative dynamics of marine ice sheets. Ice in the Climate System, ed. by W. R. PELTIER. Berlin, Springer-Verlag, 67-99 (NATO ASI Series I(12)).

HUTTER, K. (1983): Theoretical Glaciology. Dordrecht, D. Reidel, 510p.

HUYBRECHTS, P. (1990): A 3-D model for the Antarctic ice sheet: A sensitivity study on the glacial-interglacial contrast. Clim. Dyn., **5**, 79–92.

HUYBRECHTS, P. (1992): The Antarctic ice sheet and environmental change: A three-dimensional modeling study. Ber. Polarforsch., **99**, 1–241.

HUYBRECHTS, P. (1993): Glaciological modeling of the Late Cenozoic East Antarctic ice sheet: Stability or dynamism? Geogr. Ann., **75** A(4), 221–238.

HUYBRECHTS, P. and OERLEMANS, J. (1988): Evolution of the East Antarctic Ice Sheet: A numerical study of thermo-mechanical response patterns with changing climate. Ann. Glaciol., **11**, 52–59.

JENSSEN, D. (1977): A three-dimensional polar ice-sheet model. J. Glaciol., **18** (80), 373–389.

JOUZEL, J. and MERLIVAT L. (1984): Deuterium and oxygen 18 in precipitation: Modeling of the isotopic effects during snow formation. J. Geophys. Res., **89** (D7), 11749–11757.

JOUZEL, J., LORIUS, C., PETIT, J.R., GENTHON, C., BARKOV, N.I., KOTLYAKOV, V.M. and PETROV, V.M. (1987): Vostok ice core: A continuous isotope temperature record over the last climatic cycle (160,000 years). Nature, **329**, 403–407.

KAMEDA, T., NAKAWO, M., MAE, S., WATANABE, O. and NARUSE, R. (1990): Thinning of the ice sheet estimated from total gas content of ice cores in Mizuho Plateau, East Antarctica. Ann. Glaciol., **14**, 131–135.

KAMIYAMA, K., FURUKAWA, T., MAENO, H., KISHI, T. and KANAO, M. (1994): Glaciological data collected by the 33rd Japanese Antarctic Research Expedition in 1992. JARE Data Rep., **194**, 67p.

LORIUS, C., JOUZEL, J., RITZ, C., MERLIVAT, L., BARKOV, N.I., KOROTKEVICH, Y.S. and KOTLYAKOV, V. M. (1985): A 150,000-year climatic record from Antarctic ice. Nature, **316**, 591–596.

MAE, S. (1979): The basal sliding of a thinning ice sheet, Mizuho Plateau, East Antarctica. J. Glaciol., **24** (90), 53–61.

MAE, S. and NARUSE, R. (1978): Possible causes of ice sheet thinning in the Mizuho Plateau. Nature, **273**, 291–292.

MAE, S. and YOSHIDA, M. (1987): Airborne radio echo-sounding in Shirase Glacier Drainage Basin, Antarctica. Ann. Glaciol., **9**, 160–165.

MCMEEKING, R.M. and JOHNSON, R.E. (1985) On the analysis of longitudinal stress in glaciers. J. Glaciol., **31** (109), 293–302.

MITCHELL, A.R. and GRIFFITHS, D.R. (1980): The Finite Difference Method in Partial Differential Equations. Chisester, J. Wiley, 272p.

MORIWAKI, K. and YOSHIDA, Y. (1983): Submarine topography of Lützow-Holm Bay, Antarctica. Mem. Natl Inst. Polar Res., Spec. Issue, **28**, 247–258.

MUSZYNSKI, I. and BIRCHFIELD, G.E. (1987): A coupled marine ice-stream - ice-shelf model. J. Glaciol., **33** (113), 3–15.

NAGAO, M., NAKAWO, M. and HIGASHI, A. (1984): Computer simulation of the ice sheet in the Shirase Basin, Antarctica. Ann. Glaciol., **5**, 219–221.

NARUSE, R. (1979): Thinning of the ice sheet in Mizuho Plateau, East Antarctica. J. Glaciol., **24** (90), 45–52.

NISHIO, F. and URATSUKA, S. (1991): Subglacial water layer and grounding line derived from backscattering coefficients of radio echo sounding in the Shirase Glacier and Roi Baudouin Ice Shelf, East Antarctica. Proc. NIPR Symp. Polar Meteorol. Glaciol., **4**, 93–102.

NISHIO, F., MAE, S., OHMAE, H., TAKAHASHI, S., NAKAWO, M. and KAWADA, K. (1989): Dynamical behavior of the ice sheet in Mizuho Plateau, East Antarctica. Proc. NIPR Symp. Polar Meteorol.

Glaciol., **2**, 97–104.

PATERSON, W.S.B. (1981): The Physics of Glaciers, 2nd ed. Oxford, Pergamon Press, 380p.

PATTYN, F., HUYBRECHTS, P. and DECLEIR, H. (1989): Modeling glacier fluctuations in the Sør Rondane, Dronning Maud Land, Antarctica. Z. Gletscherkd. Glazialgeol., **25**, 33–47.

PATTYN, F., DECLEIR, H. and HUYBRECHTS, P. (1992): Glaciation of the central part of the Sør Rondane, Antarctica: Glaciological evidence. Recent Progress in Antarctic Earth Science, ed. by Y. YOSHIDA *et al.* Tokyo, Terra Sci. Publ., 669–678 .

PRESS, W.H., TEUKOLSKY, S.A., VETTERLING, W.T. and FLANNERY, B.P. (1992): Numerical Recipes in C: The Art of Scientific Computing, 2nd ed. Cambridge, Cambridge University Press, 994p.

RITZ, C. (1987): Time dependent boundary conditions for calculation of temperature fields in ice sheets. The Physical Basis of Ice sheet Modeling, ed. by E. D. WADDINGTON and J. S. WALDER. Wallingford, IAHS Press, 207-216 (IAHS Publication, No. 170).

RITZ, C. (1989) Interpretation of the temperature profile measured at Vostok, East Antarctica. Ann. Glaciol., **12**, 138–144.

SATOW, K. and KIKUCHI, T. (1995): The 10 m snow temperature in the ice sheet. Antarctica, East Queen Maud Land, Enderby Land; Glaciological Folio, ed. by A. HIGASHI. Tokyo, Natl Inst. Polar Res.

SCLATER, J.G., JAUPART, C. and GALSON, D. (1980): The heat flow through oceanic and continental crust and the heat loss of the earth. Rev. Geophys. Space Phys., **18**, 289–311.

SHACKLETON, N.J. (1987): Oxygen isotopes, ice volume and sea level. Quat. Science Rev., **6**, 183–190.

TAKAHASHI, S. and WATANABE, O. (1995): Snow accumulation (surface mass balance). Antarctica, East Queen Maud Land, Enderby Land; Glaciological Folio, ed. by A. HIGASHI. Tokyo, Natl Inst. Polar Res.

THOMAS, R.H. (1973): The creep of ice shelves. J. Glaciol., **12** (64), 45–53.

TOH, H. and SHIBUYA, K. (1992): Thinning rate of ice sheet on Mizuho Plateau, East Antarctica, determined by GPS differential positioning. Recent Progress in Antarctic Earth Science, ed. by Y. YOSHIDA *et al.* Tokyo, Terra Sci. Publ., 579–583.

VAN DER VEEN, C.J. (1987): Longitudinal stress and basal sliding: a comparative study. Dynamics of the West Antarctic Ice Sheet, ed. by C.J. VAN DER VEEN, and J. OERLEMANS. Dordrecht, D. Reidel, 223 –248.

VAN DER VEEN, C.J. and WHILLANS, I.M. (1989): Force budget: I. Theory and numerical methods. J. Glaciol., **35** (119), 53–60.

WATANABE, O., FUJII, Y., NISHIO, F. and MOTOYAMA, H. (1992): Position, elevation, ice thickness and bedrock elevation of stations along the routes in East Queen Maud Land and Enderby Land, East Antarctica. JARE Data Rep., **180**, 143p.

(Received January 30, 1995; Revised manuscript received June 12, 1995)